

Article

Dynamic and Thermal Properties of Aluminum Alloy A356/Silicon Carbide Hollow Particle Syntactic Foams

James Cox ¹, Dung D. Luong ¹, Vasanth Chakravarthy Shunmugasamy ¹, Nikhil Gupta ^{1,*}, Oliver M. Strbik III ² and Kyu Cho ³

¹ Composite Materials and Mechanics Laboratory, Mechanical and Aerospace Engineering Department, Polytechnic School of Engineering, New York University, Brooklyn, NY 11201, USA; E-Mails: jc5430@nyu.edu (J.C.); ddl268@nyu.edu (D.D.L.); vs860@nyu.edu (V.C.S.)

² Deep Springs Technology, LLC, 4750 W. Bancroft St., Toledo, OH 43615, USA; E-Mail: ostrbik@teamdst.com

³ U.S. Army Research Laboratory, RDRL-WMM-D, Aberdeen Proving Ground, MD 21005-5069, USA; E-Mail: kyu.c.cho2.civ@mail.mil

* Author to whom correspondence should be addressed; E-Mail: ngupta@nyu.edu; Tel.: +1-646-997-3080; Fax: +1-646-997-3532.

External Editor: Hugo F. Lopez

Received: 8 August 2014; in revised form: 27 November 2014 / Accepted: 27 November 2014 / Published: 2 December 2014

Abstract: Aluminum alloy A356 matrix syntactic foams filled with SiC hollow particles (SiC_{HP}) are studied in the present work. Two compositions of syntactic foams are studied for quasi-static and high strain rate compression. In addition, dynamic mechanical analysis is conducted to study the temperature dependent energy dissipation and damping capabilities of these materials. The thermal characterization includes study of the coefficient of thermal expansion (CTE). A356/SiC_{HP} syntactic foams are not strain rate sensitive as the compressive strength displayed little variation between the tested strain rates of 0.001–2100 s⁻¹. Microscopic analysis of the high strain rate compression tested specimens showed that the fracture is initiated by the failure of hollow particles at the onset of the plastic deformation region. This is followed by plastic deformation of the matrix material and further crushing of particles. The syntactic foams showed decrease in storage modulus with increasing temperature and the trend was nearly linear up to 500 °C. The alloy shows a similar behavior at low temperature but the decrease in storage modulus increases sharply over 375 °C. The loss modulus is very small for the tested materials

because of lack of viscoelasticity in metallic materials. The trend in the loss modulus is opposite, where the matrix alloy has lower loss modulus than syntactic foams at low temperature. However, over 250 °C the matrix loss modulus starts to increase rapidly and attains a peak around 460 °C. Syntactic foams have higher damping parameter at low temperatures than the matrix alloy. Incorporation of SiC_{HP} helps in decreasing CTE. Compared to the CTE of the matrix alloy, $23.4 \times 10^{-6} \text{ }^\circ\text{C}^{-1}$, syntactic foams showed CTE values as low as $11.67 \times 10^{-6} \text{ }^\circ\text{C}^{-1}$.

Keywords: metal matrix syntactic foam; SiC hollow particle; high strain rate compression; damping parameter

1. Introduction

Syntactic foams are hollow particle filled composite materials that are classified as closed-cell foams. Presence of hollow particles provides these materials with a set of unique properties which include sufficiently high strength to enable structural applications, large densification strain that results in high energy absorption capability, and low coefficient of thermal expansion (CTE) leading to better dimensional stability. The wall thickness, volume fraction, and bulk density of hollow particles can be used to tune properties of syntactic foams [1–5]. Methods used for synthesizing particle reinforced metal matrix composites (MMCs) can be adapted to synthesize metal matrix syntactic foams (MMSFs).

Lightweight but stronger materials can reduce the weight of automotive structures, which translates into reduced fuel consumption and emissions. Lightweight syntactic foams are candidate materials for several components in automobiles and other modes of transportation [6]. Due to the ability of syntactic foams to absorb large amounts of compressive energy, they are used in automotive crash structures. In addition, this weight saving can lead to increased payload capacity in aerospace and marine applications [7–9]. Aluminum and magnesium matrix syntactic foams have been extensively studied in the recent literature [3,10]. Syntactic foams of heavier metals and alloys such as iron [11,12], Invar [11], titanium [13,14], and zinc [15] have also been studied because the reduced density of these materials can enable weight saving in their existing applications. Most of these studies have used fly-ash cenospheres and hollow particles of ceramics such as SiC or Al₂O₃ as fillers.

Several studies are available on compressive properties of aluminum matrix syntactic foams (AMSFs). A356 alloy has been used with expanded perlite particles to synthesize very low density (1.05 g/cm³) syntactic foams. The plateau strength of as-cast and heat treated syntactic foams varied between 29 and 52 MPa [16]. A356/alumina hollow particle syntactic foams did not show strain rate sensitivity in compressive properties. The foam with higher density or hollow particle wall thickness had higher compressive properties [17]. Studies of A356/alumina and A2014/cenosphere filler syntactic foams showed that under compression, syntactic foams develop shear zones along which particles fracture and densify. The size of the densification zone increases with compressive strain and results in the stress plateau seen in the stress-strain diagrams of these materials [17–19]. Similar features are observed in the compression testing of pure Al/alumino-silicate hollow sphere

AMSFs [20]. Al 1100 and Al 6061 alloy matrix AMSFs are also found studied and the results show that the precipitation strengthening mechanism in Al 6061 alloy helps in improving the properties of syntactic foams compared to other alloy systems [21]. Heat treatment is found to have a remarkable effect on the compressive properties of A206/alumina syntactic foams [22]. Al 7075 matrix tested under impact loading conditions showed 20%–30% higher plateau stress compared to that under quasi-static compressive condition [23]. The results of this study indicate some effect of strain rate on the material. However, difference in the impact and static compressive loading test methods can also lead to some difference in the results obtained through these methods. In testing a multilayer structure containing Al 6061/cenosphere syntactic foam sandwiched between solid aluminum and steel specimen, it was concluded that the syntactic foam showed strain rate sensitivity at 2650 and 3350 s⁻¹ strain rates compared to the quasi-static values [24].

Compared to the vast amount of literature available on the compressive properties of AMSFs, only one study was found on the dynamic mechanical analysis (DMA) [17]. One of the main reasons for this lack of studies may be that DMA relies on measuring damping properties of materials, which are mainly contributed by viscoelasticity. Metals do not show viscoelastic behavior at low temperatures. However, the response of metals at high temperatures can be different. In addition, inclusion of ceramic particles is expected to improve their thermal stability compared to the matrix alloy and make a difference in their high temperature behavior. Therefore, it is important to analyze the high temperature dynamic properties of MMSFs. The CTE of AMSFs is also scarcely studied [25]. Al/fly ash syntactic foams were found to have lower CTE than that of the matrix alloy. Numerical studies on CTE are available mainly for polymer matrix syntactic foams, which can be generalized to AMSFs because the simulations are conducted using only elastic constitutive models [26]. However, at high temperature, the possibility of phase transformation, precipitate dissolution, oxidation, change in the particle-matrix interface structure, and diffusion are neglected in these studies, which can be relevant to AMSFs.

In the present work, A356 matrix SiC hollow particle (SiC_{HP}) filled syntactic foams are studied for quasi-static and high strain rate compression, thermal expansion, and dynamic mechanical properties. Extensive failure analysis is conducted through microscopy to understand the failure mechanisms under compressive loading conditions at different strain rates. Studies focusing on the compressive properties of aluminum/SiC syntactic foams are available and the results of the present work are compared with the existing results. High temperature damping, energy storage and dissipation capabilities are important for such materials in predicting their service life and limits.

2. Materials and Methods

2.1. Materials

A356 alloy is used to synthesize syntactic foams by using a pressureless infiltration method in a bed of hollow SiC particles [17]. In the present work, two sample types were studied, which are referred to as S1 and S2 types and had measured densities of 1.71 ± 0.06 and 1.84 ± 0.03 (g/cm³), respectively. The mean particle diameter is 1 mm for both particle types while the wall thickness for particles used in sample types S1 and S2 are 67.8 ± 13.6 and 79.3 ± 20.5 μm, respectively. The density of syntactic

foams is calculated by measuring the dimensions and weight of compression test specimens. The SiC_{HP} volume fractions for both syntactic foam types were approximately 60%. The true particle densities of these SiC_{HP} cannot be measured because of porosity in their walls [27]. The porosity in the walls results in having lower mechanical properties compared to SiC particles that have the same true particle density but have fully dense walls.

2.2. Quasi-Static Compression

The quasi-static compression testing was conducted using an Instron 4469 test system equipped with a 50 kN load cell. Bluehill 2.0 software (Instron Inc., Norwood, MA, USA) was used for acquisition of load and displacement data. Three different specimens were tested at strain rates of 10^{-2} s^{-1} and 10^{-4} s^{-1} . A thin layer of grease was applied during compression to avoid specimen barreling effect due to friction. The cylindrical test specimens had a nominal diameter of 10 mm and thickness of 5 mm. The same specimen dimensions were maintained for the quasi-static and high strain rate compression tests, so that the results can be directly compared.

2.3. High Strain Rate Compression

The high strain rate compression (HSR) test was conducted using an in-house developed split-Hopkinson pressure bar (SHPB) setup, in the strain rate range of 800–2100 s^{-1} . A cylindrical specimen is placed between the two long slender bars, called the incident and transmitter bars. Grease is applied to both ends of the specimen. Strain pulse signals from the incident and transmitter bars are collected using strain gauges. Considering one-dimensional wave propagation in the bars, the strain rate, stress, and strain in the specimen can be calculated by

$$\dot{\varepsilon}(t) = \frac{2C_b \varepsilon_r(t)}{l_0} \quad (1)$$

$$\sigma(t) = \frac{AE \varepsilon_r(t)}{A_0} \quad (2)$$

$$\varepsilon(t) = \int_0^t \dot{\varepsilon}(t) dt \quad (3)$$

where A and E are the cross sectional area and Young's modulus, respectively, of the incident and transmitted bar material and c_b is the sound wave velocity in the bar. The constants l_0 and A_0 are the initial length and cross sectional area of the specimen, respectively. The variable t represents time, $\varepsilon_r(t)$ and $\varepsilon(t)$ are the reflected and transmitted axial strain pulses, respectively. The details of the test instrumentation and calculation procedure have been published elsewhere [28,29]. In this work, incident, transmitted, and striker bars of Inconel alloy were used. The Young's modulus and density of the Inconel alloy used in the calculations were 195 GPa and 8400 kg/m^3 , respectively. The length and diameter of the incident and transmitted bars were 1.83 m and 12.7 mm, respectively.

2.4. Failure Analysis

The failure analysis was conducted using a Hitachi S-3400N (Tarrytown, NY, USA) variable pressure scanning electron microscope (SEM), which is equipped with secondary electron and backscattered electron detectors. The specimens were sputter coated with gold before the SEM observation using Leica EM SCD050 (Leica Microsystems Inc., Buffalo Grove, IL, USA).

2.5. Dynamic Mechanical Analysis

A Q800 (TA Instruments, New Castle, DE, USA) dynamic mechanical analyzer (DMA) was used to test the specimens at a constant frequency of 1 Hz in the temperature range of 35–510 °C under three-point bend configuration. A static force of 1 N was applied at the mid-point of the specimen and the span length was fixed at 50 mm. The nominal dimensions of the syntactic foam specimens were 10.5 mm width and 3.5 mm thickness. The pins were roller supported type to provide uniform loading on the material and to inhibit friction effects.

2.6. Thermo-Mechanical Analysis

The coefficient of thermal expansion (CTE) was determined using a Q400 thermo-mechanical analyzer (TA Instruments, New Castle, DE, USA). The specimens were tested from an initial temperature of 35 °C–405 °C at the ramp rate of 10 °C/min. A preload of 0.05 N was applied. The specimens had a nominal height and diameter of 10.5 and 10.0 mm, respectively. The glass probe which measures the dimensional change and applies the preload on the specimen was placed directly at the center on the top surface of the specimens. The CTE (α) was determined by

$$\alpha = \frac{1}{l_0} \frac{dl}{dt} \quad (4)$$

where l_0 is the initial specimen height and t is time and dl/dt denotes the slope of the change in specimen height over change in temperature.

3. Results and Discussion

3.1. Microstructure

Extensive microscopy was conducted on several specimens in the as-synthesized condition. Figure 1 shows the microstructure of a randomly selected S1 type AMSF specimen. A continuous interface is observed between particles and the matrix. It is observed that the SiC_{HP} have porous walls. Such particles have been previously studied in detail through microscopy and single particle compression method [27]. The porosity in the wall makes these particles lighter than the similar sized particles that have fully dense walls. However, it also results in lower strength in these particles than that expected from particles of the same material having fully dense walls [30]. Similar features are observed for S2 specimens in Figure 2. The SiC_{HP} hollow particle can be seen well dispersed in both specimens. The micrographs show that the particles survive the composite synthesis process. The layer of matrix alloy between closely spaced hollow particles shows good wetting at the matrix particle

interface, which can provide high interfacial strength and mechanical interlocking between the particles and matrix material.

Figure 1. SiC_{HP} reinforced AMSFs of type S1: (a,b) secondary electron and (c) backscattered electron detector image. Images (b) and (c) are obtained from the region marked with dotted ellipse in (a).

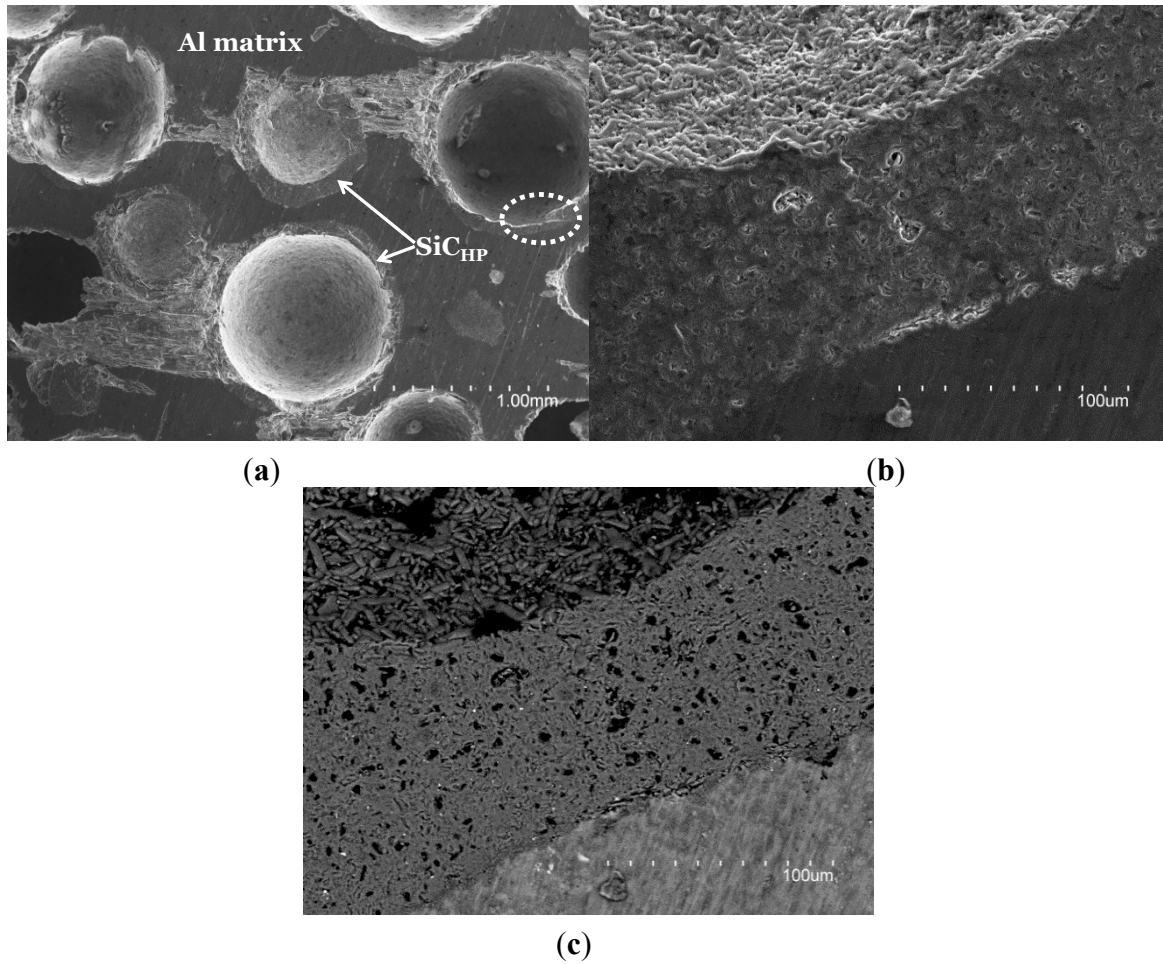


Figure 2. SiC_{HP} reinforced AMSFs of type S2: (a,b) secondary electron and (c) backscattered electron detector image. Images (b) and (c) are obtained from the region marked with dotted ellipse in (a).

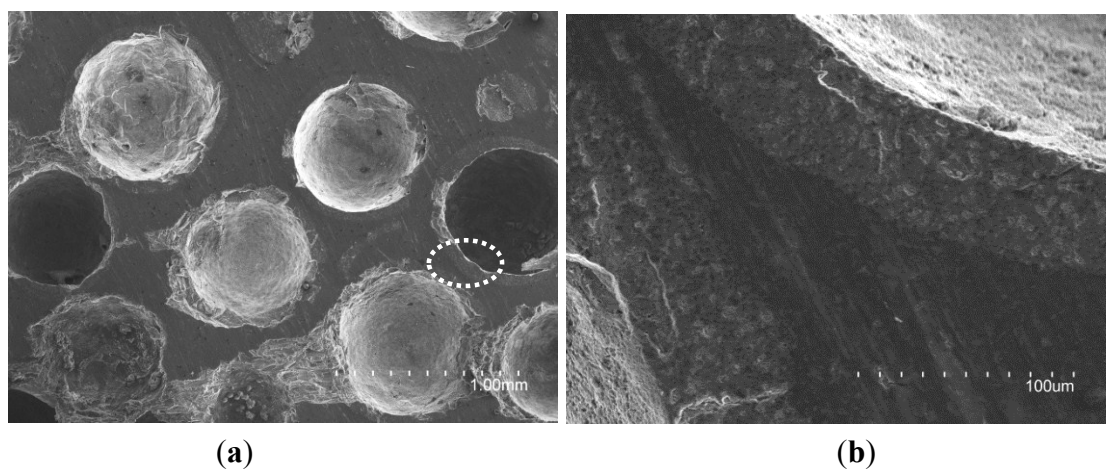
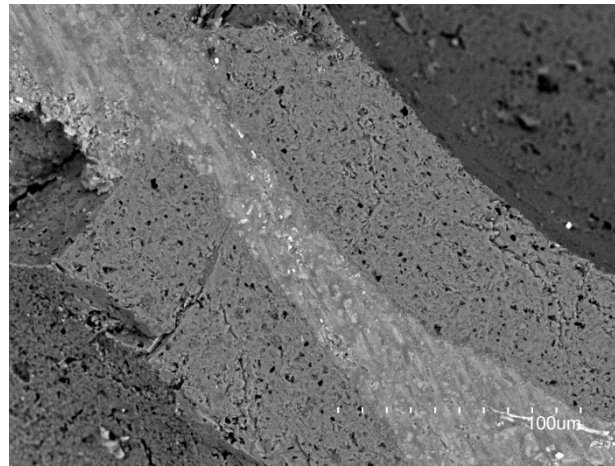


Figure 2. Cont.

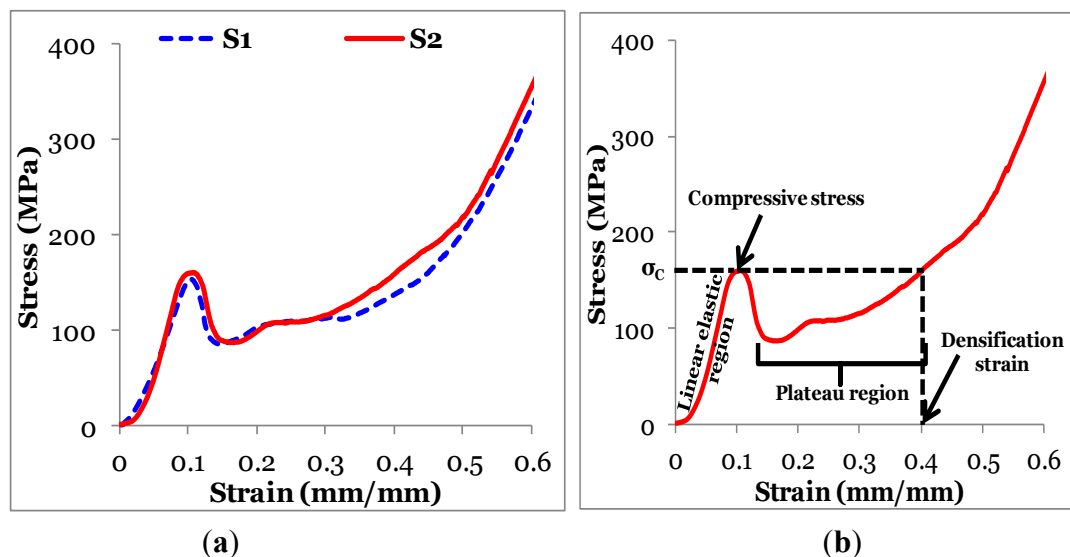


(c)

3.2. Quasi-Static Compression

The stress–strain relation for a representative specimen of each sample types can be seen in Figure 3. These graphs are qualitatively similar to those previously observed for A356 matrix syntactic foams containing SiC_{HP} or Al₂O_{3-HP} fillers [9,17]. The curves show an initial linear elastic region at the end of which the stress drops sharply due to onset of particle failure. The stress becomes relatively constant over a large strain range, known as the plateau region. In this region, particle crushing and foam compaction take place. Following the plateau region, the stress begins to rise again as the material densification completes [18,20,31,32]. These graphs are used to calculate the compressive strength of syntactic foams, which is defined as peak stress following the linear elastic region, plateau strength and densification strain.

Figure 3. (a) A set of representative quasi-static compressive stress-strain graphs of A356/SiC_{HP} syntactic foams and (b) stress-strain curve of S2 specimen showing the linear elastic region, compressive stress, plateau region and the densification strain.



The quasi-static compression results for the S1 and S2 syntactic foams are summarized in Table 1. Both sample types showed no difference in mechanical properties between the two strain rates of 10^{-2} s^{-1} and 10^{-4} s^{-4} , thus the results are combined for both strain rates in Table 1. The S1 type had a compressive strength and specific compressive strength of 152.4 MPa and 89.1 MPa/(g/cm³) respectively, while the S2 type had a compressive strength and specific compressive strength of 161.1 MPa and 87.4 MPa/(g/cm³), respectively. The S2 type has a higher compressive strength when compared to the S1 type, yet due to its higher density it has a lower specific compressive strength. However, the standard deviations overlap for the two composites so this trend cannot be strongly identified from the results. Having the densities of both composites only slightly different contributes to the overlapping trends. It is also observed that S1 and S2 AMSFs have plateau stress of 103.0 and 109.0 MPa, respectively. These results show that the syntactic foam having higher density has higher compressive strength and plateau strength.

Table 1. Quasi-static compressive properties of A356/SiC_{HP} syntactic foams.

Sample type	Measured density (g/cm ³)	Compressive strength (MPa)	Specific compressive strength (MPa/(g/cm ³))	Plateau stress (MPa)	Densification strain (mm/mm)
S1	1.71 ± 0.06	152.4 ± 4.3	89.1 ± 2.0	103.0 ± 7.2	0.44 ± 0.01
S2	1.84 ± 0.03	161.1 ± 7.8	87.4 ± 4.3	109.0 ± 4.1	0.41 ± 0.02

Previous studies have also shown that aluminum is not strain rate sensitive [9], especially at such low strain rates. The strain rate insensitivity is related to the crystal structure of aluminum, which is face centered cubic (FCC). The FCC crystals contain close-packed plains and 12 slip systems. The activation energy for slip on the close-packed plains is relatively lower compared to planes having lower atomic densities. Hence, the strain rate sensitivity is not observed in most FCC metals at low strain rates. The precipitates and grain boundaries present in the material microstructure may result in some strain rate sensitivity at high strain rate.

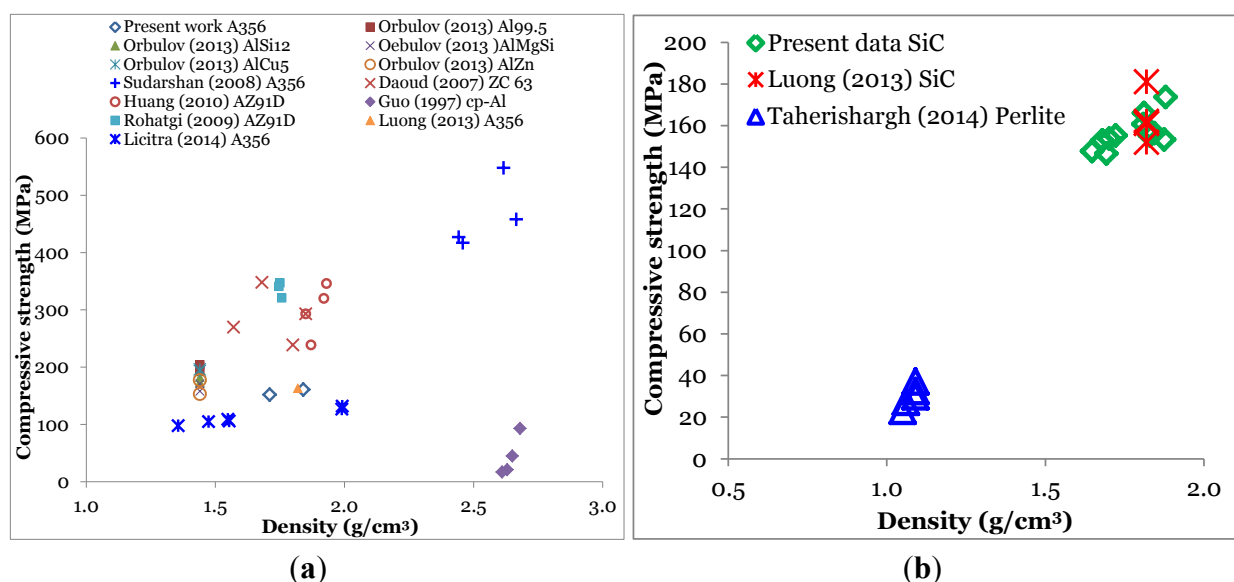
The densification strain was taken as the point where the stress after the plateau region equals the compressive strength. The densification strains of S1 and S2 syntactic foams were 0.44 and 0.41 mm/mm, respectively. The S2 syntactic foam contains thicker walled particles, hence, lower porosity in the denser specimen likely results in smaller densification strain.

Several observations made in the published literature can provide additional insight into the behavior of AMSFs. Some of the relevant observations are summarized here. Orbulov *et al.* reported that the mechanical properties of AMSFs can be tailored by mixing different material types of hollow particles, thus creating a hybrid syntactic foam [33]. Rocha Rivero *et al.* studied the effect of matrix strength and reported that the peak strength, plateau strength, and toughness of the syntactic foam increased with the increase of yield stress of the matrix material [34].

A comparison of the results obtained from the present work and the literature data is presented in Figure 4, where Figure 4a includes different types of alloys and Figure 4b includes only the available results on syntactic foams using A356 alloy [9,17,35–40]. Many different types of particles have been used in these studies with metallic matrices. It is observed in both Figure 4a,b that most of the data are located in a narrow band with a clear trend that the higher density foams have higher strength. Within syntactic foams of one alloy, heat treatments are found to be effective in increasing the strength

without affecting the density. Comparing the results of A356 alloy syntactic foams, it could be observed that fly ash cenosphere fillers show the highest strength. However, control over the size and wall thickness of fly ash cenospheres is difficult. Ceramic hollow spheres are a good alternative to fly ash; however, availability of high quality ceramic particles with defect-free walls can also help in producing syntactic foams with higher performance. It should also be noted that a large number of studies have been conducted in the past three years, which demonstrates increasing interest in such lightweight materials for industrial applications.

Figure 4. (a) Comparison of results obtained from the present study with literature data on aluminum and magnesium matrix syntactic foams. The studies use different types of alloys and hollow particles [9,17,35–40]. (b) Studies comparing results only on A356 alloy matrix syntactic foams [9,16].



3.3. High Strain Rate Compression

The stress–strain trend at HSR compression is qualitatively similar to the quasi-static compression. However, the end of the HSR compression test may not mark complete densification because the time duration of the test depends on the pulse length obtained in the SHPB test instrumentation. HSR compression test results are summarized in Figure 5. It is observed in Figure 5a that the syntactic foams do not show any measurable strain rate sensitivity. Syntactic foams have been tested in the strain rate range of 800–2100 s⁻¹ as observed in Figure 5a. The compressive strength over the entire set of high strain rates is found to be 138.8 ± 4.5 and 139.5 ± 5.3 MPa for S1 and S2 syntactic foams, respectively. The HSR strength values are 8.9% and 13.3% lower than the quasi-static compressive strength values for S1 and S2 foams, respectively. The small difference with partially overlapping standard deviations does not provide evidence of strain rate sensitivity in the A356/SiC_{HP} syntactic foams under HSR compression.

Figure 5. (a) Compressive strength and (b) specific strength represented with respect to strain rate, for different syntactic foams types, where the strain rate axis is plotted on logarithmic scale. The inset images show the same HSR data plotted on a normal scale [9].

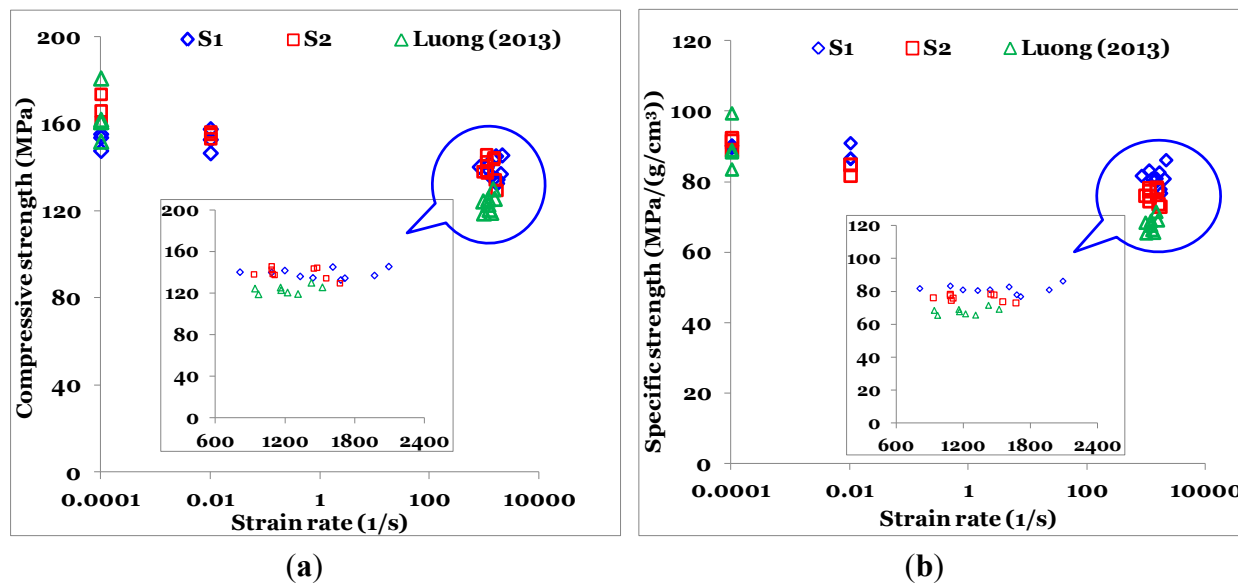


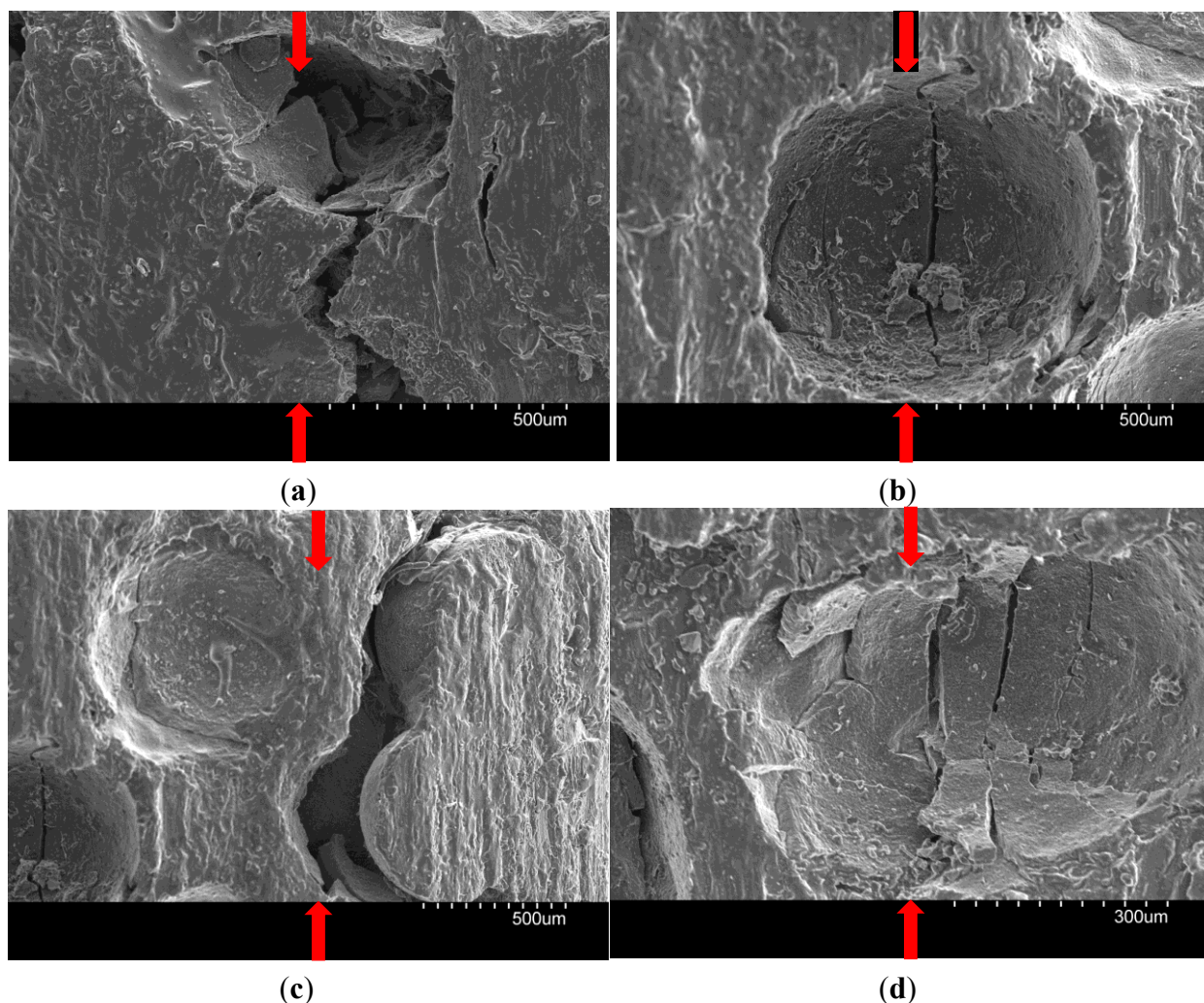
Figure 5 also shows results from a previous study on A356/SiC_{HP} syntactic foam containing a different particle size and volume fraction [9]. The results of the previous study and of the current work show similar trends. However, the conclusion that A356/SiC_{HP} syntactic foam is not strain rate sensitive within the quasi-static and high strain rate regimes is limited to the strain rates used in the present work, which span from 0.001–2100 s⁻¹. Several existing studies are focused on strain rate sensitivity of aluminum syntactic foams with different types of particles [7,8,41]. Dou *et al.* report strain rate sensitivity for cenosphere-pure aluminum syntactic foams, for strain rates ranging from quasi-static to 5000 s⁻¹ [41]. They observed complete densification of the cenosphere-pure aluminum syntactic foams.

The specific compressive strength is shown in Figure 5b. The specific compressive strength for the S1 and S2 type syntactic foams was measured as 81.2 and 76.1 MPa/(g/cm³), respectively. The strain rate insensitivity of the A356/SiC_{HP} syntactic foams makes them useful for application in crash structures, as the identical mechanical properties along varying strain rates is ideal for structures that could be subjected to a wide range of impact intensities since their energy absorption capability can be predicted by simple quasi-static tests.

The micrographs of a representative specimen tested at 1700 s⁻¹ strain rate are presented in Figure 6. Arrows indicate the loading direction relative to the orientation of the image. These micrographs reveal that the HSR test resulted in cracking of SiC_{HP} in the loading direction. Figure 6 also shows hollow particle crushing and plastic deformation of the matrix material. The fracture mechanism of A356/SiC_{HP} syntactic foams has been documented in detail in previous studies [9]. It is noted that the failure of the material starts at the peak stress at the end of the elastic region in the form of particle cracking. However, subsequent compression results in formation of macroscopic deformation bands in the specimens along the shear directions, which result in plastic flow of metal and shear failure of particles. The growth of these shear zones results in complete densification of the material and

constitutes final failure. The extent of densification in HSR testing depends on the compressive strain obtained in the SHPB instrumentation. These failure mechanisms are similar for quasi-static and HSR compression in the strain rate range tested in the present study. There is no indication of particle–matrix interfacial failure under either quasi-static or HSR compression.

Figure 6. Failure features of S1 type AMSFs after compression at a strain rate of 1700 s^{-1} . Arrows indicates the loading direction. (a,c) Cracks in the matrix alloy, (b,d) cracking of particles in the direction of compression. Since the failure strain at HSR compression is small, the shear failure signs are not clearly observed in these figures.



3.4. Dynamic Mechanical Analysis

Although the energy absorption and damping capabilities are important for many applications, these properties have not been widely studied for metal matrix syntactic foams. There is a very limited amount of literature available concerning DMA for particulate MMCs, particularly on SiC reinforced MMCs [36,42–44]. DMA can measure the stiffness and damping of a material over a large range of temperatures and loading frequencies. The results of DMA testing are shown in Figure 7, where graphs present storage modulus and loss modulus with respect to temperature. The results of A356 alloy are taken from a recent study [17]. Both syntactic foams show similar behavior for storage and loss

moduli. Syntactic foams show a decrease in storage modulus as the temperature increases in Figure 7a. The storage modulus-temperature profile is nearly linear for syntactic foams in the test temperature range. In comparison, the alloy shows a bilinear curve with respect to temperature. There is a steep decrease in storage modulus above 375 °C. The results show that the storage modulus of alloy is higher than that of the syntactic foams but the difference decreases rapidly after the transition temperature. The loss modulus shows an opposite trend in Figure 7b. The loss modulus increases with temperature. It is observed that the loss modulus of the alloy is comparable to that of syntactic foams at low temperature. However, at temperatures above 250 °C the loss modulus of the alloy starts to increase rapidly and shows a peak around 460 °C. Syntactic foams show a more stable thermal behavior and do not show evidence of a peak within the test temperature range. The ratio of loss to storage modulus is defined as the damping parameter $\tan\delta$. The damping parameter of syntactic foams is higher than that of the alloy at temperatures below about 425 °C as observed in Figure 8. Above this temperature, the damping parameters of composites and the alloy become nearly the same. The porosity in the walls of particles is expected to help in obtaining higher damping the syntactic foams. The values of storage modulus, loss modulus and $\tan\delta$ are extracted from the graphs at three different temperatures of 50, 200 and 400 °C and are presented in Table 2. These temperatures are arbitrarily selected to cover different trends and observe the difference in values. The properties can be extracted at any other temperature of interest based on the applications of these materials. There are some important trends to note in this table. It is observed that the due to a lack of viscoelasticity in aluminum alloy, the storage modulus is nearly the same as the elastic modulus. It is also observed in that the loss modulus is negligible compared to the storage modulus. The value of the loss modulus for the A356 alloy is only 1.4% compared to the storage modulus at 50 °C. The damping parameter $\tan\delta$ is also negligible at 50 °C. As the temperature is increased, the stiffness of the material decreases, which is reflected as the reduced storage modulus. Correspondingly, the loss modulus increases. At 400 °C the value of the loss modulus for the alloy is 12% compared to the storage modulus and $\tan\delta$ increased by a factor of 8.6 compared to the value at 50 °C.

Figure 7. (a) Storage modulus and (b) loss modulus with respect to temperature for the two different types of syntactic foams and also for the matrix alloy.

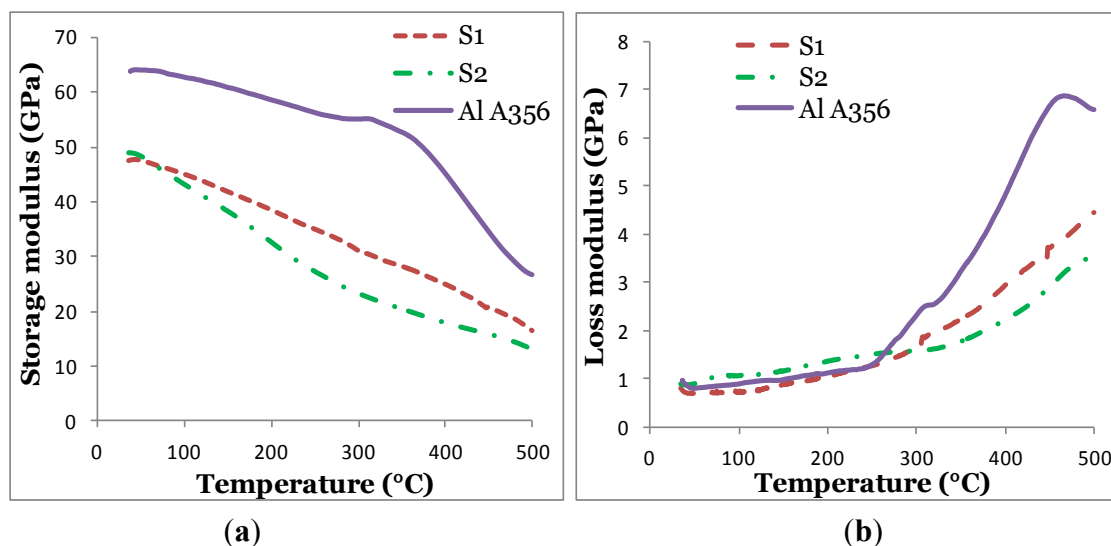


Figure 8. Damping parameter $\tan \delta$ with respect to temperature for the two different types of syntactic foams and also for the matrix alloy.

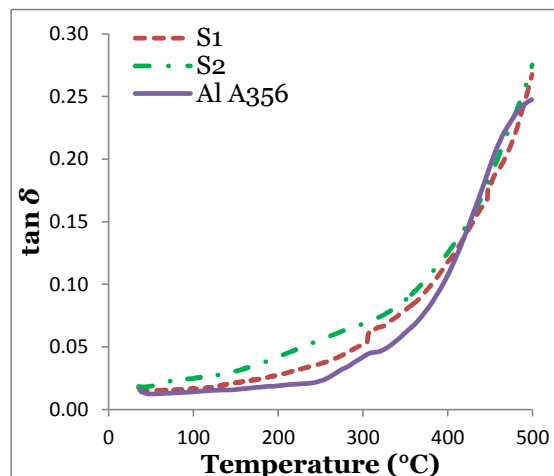


Table 2. Dynamic properties of A356/SiC_{HP} syntactic foams at different temperatures.

Sample	Storage modulus (GPa)	Loss modulus (GPa)	$\tan \delta$
	(50, 200, 400 °C)	(50, 200, 400 °C)	(50, 200, 400 °C)
S1	47.45, 37.69, 25.79	0.70, 1.04, 3.22	0.015, 0.028, 0.125
S2	48.88, 32.57, 17.84	0.90, 1.39, 2.40	0.018, 0.043, 0.134
A356	69.22, 63.42, 48.07	0.98, 1.19, 5.79	0.014, 0.019, 0.120

Similar changes are observed in the properties of syntactic foams. Difference in the stiffness of the particle and matrix material is expected to help in providing damping at high temperatures by causing deformation along the particle-matrix interface.

Figure 9 shows micrographs of a specimen after DMA testing. Cracks in the SiC_{HP} can be observed in this figure after the testing. Oxide layer formation on the aluminum alloy matrix also takes place due to high temperature during the testing.

A representative thermal strain curve with respect to temperature is shown in Figure 10 for a randomly selected S1 syntactic foam specimen. The curve shows two different linear regions, so the CTE values are calculated in temperature ranges of 100–200 °C and 300–400 °C. The results are summarized in Table 3 for CTE values of A356/SiC_{HP} syntactic foams. The percent change from the lower temperature range to the higher temperature range is 40.1% and 38.7% for the S1 and S2 sample types, respectively. The S1 and S2 type AMSFs had average CTE values of 14.60 ± 0.91 and 15.74 ± 0.70 ($\times 10^{-6} \text{ }^\circ\text{C}^{-1}$), respectively. Comparing the CTE value of $23.4 \times 10^{-6} \text{ }^\circ\text{C}^{-1}$ for the A356 alloy [45] with those of the two syntactic foams, it is clear that the addition of SiC_{HP} into the matrix resulted in a lower CTE.

Figure 9 do not show interfacial failure between particle and matrix, likely due to the surface porosity on the SiC_{HP} leading to mechanical bonding between particle and the matrix.

3.5. Thermomechanical Analysis

A representative thermal strain curve with respect to temperature is shown in Figure 10 for a randomly selected S1 syntactic foam specimen. The curve shows two different linear regions, so the

CTE values are calculated in temperature ranges of 100–200 °C and 300–400 °C. The results are summarized in Table 3 for CTE values of A356/SiC_{HP} syntactic foams. The percent change from the lower temperature range to the higher temperature range is 40.1% and 38.7% for the S1 and S2 sample types, respectively. The S1 and S2 type AMSFs had average CTE values of 14.60 ± 0.91 and 15.74 ± 0.70 ($\times 10^{-6}$ °C⁻¹), respectively. Comparing the CTE value of 23.4×10^{-6} °C⁻¹ for the A356 alloy [45] with those of the two syntactic foams, it is clear that the addition of SiC_{HP} into the matrix resulted in a lower CTE.

Figure 9. (a) Micrograph of S2 type A356/SiC_{HP} syntactic foam after DMA test. (b) The images show cracks in the SiC_{HP} wall and oxide formation on the surface of matrix surrounding the particle.

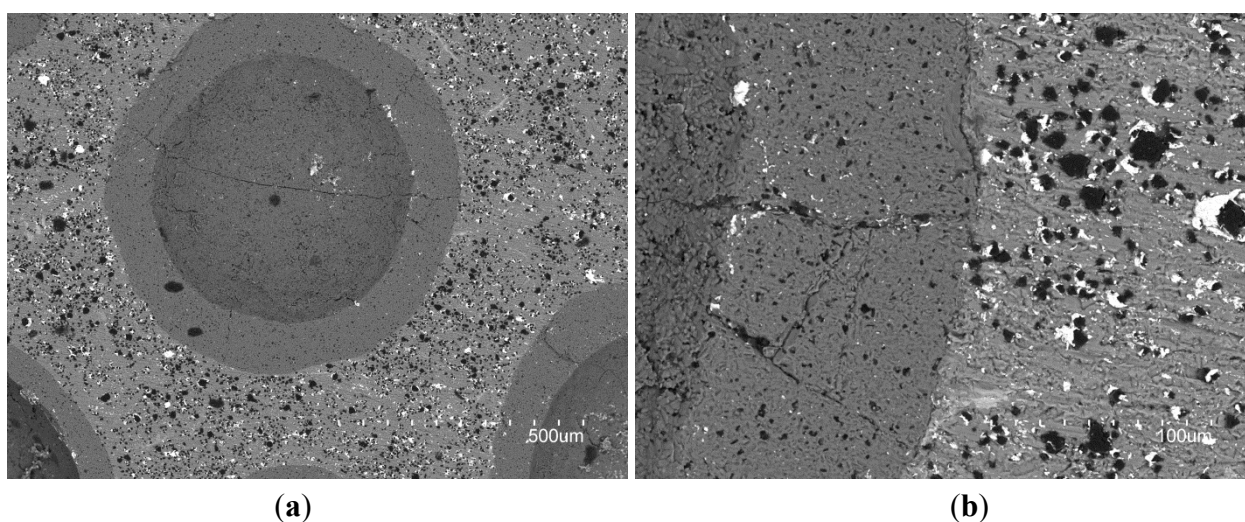


Figure 10. Thermal strain-temperature response for one specimen of S1 syntactic foam.

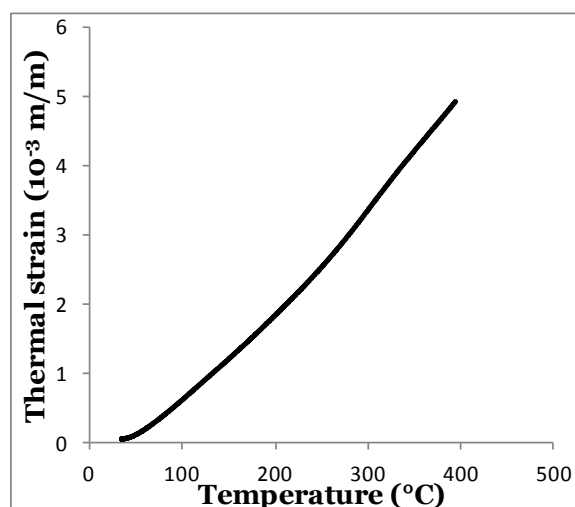


Table 3. Coefficient of thermal expansion values of the A356/SiC_{HP} syntactic foams.

Sample	CTE (100–200 °C) ($\mu\text{m}/\text{m}^\circ\text{C}$)	CTE (300–400 °C) ($\mu\text{m}/\text{m}^\circ\text{C}$)	Mean CTE ($\mu\text{m}/\text{m}^\circ\text{C}$)
S1	11.67 ± 0.42	16.35 ± 0.66	14.60 ± 0.91
S2	12.70 ± 0.36	17.61 ± 0.40	15.74 ± 0.74

Previous studies have also noted that syntactic foams have a significantly lower CTE compared to the matrix material. A similar level of CTE reduction in commercially pure AMSFs containing fly ash cenospheres was observed [25]. Fly ash particles are primarily composed of alumina, silica, and iron oxides. These ceramic particles reduced the CTE of aluminum from $25.3 \times 10^{-6} \text{ }^\circ\text{C}^{-1}$ to $11 \times 10^{-6} \text{ }^\circ\text{C}^{-1}$ [25]. Labella *et al.* reported up to 67% decrease in CTE compared to that of polymer matrix material for 60 vol. % fly ash cenosphere filled vinyl ester matrix syntactic foams [46]. For particulate MMCs, the CTE of the composite was found to increase with prestraining of the matrix [47]. It was also observed that increase of particle content decreased the CTE of particulate MMCs [47]. Elomari *et al.* reported that the CTE of the composite is dependent on a range of mechanisms from plastic yielding to volume fraction of the fractured and broken particles [47].

4. Conclusions

Aluminum alloy matrix SiC hollow particle reinforced (A356/SiC_{HP}) syntactic foams are studied in the present work for quasi-static, dynamic, and thermal properties. The A356/SiC_{HP} AMSFs were manufactured in two different densities using SiC_{HP} of different wall thicknesses. These syntactic foams are referred to as S1 and S2 type syntactic foams in this study. The following conclusions are drawn from the experimental results and analysis.

- The S1 and S2 type specimens had average densities of 1.71 and 1.84 g/cm³, respectively. The compressive strength of higher density foam was higher. The compressive strength of S1 and S2 syntactic foams was measured as 152.4 and 161.1 MPa, respectively.
- A356/SiC_{HP} syntactic foams did not show strain rate sensitivity in the range studied in the present work for both the S1 type and S2 type.
- The S1 and S2 type syntactic foams had specific quasi-static compressive strength of 89.1 and 87.4 MPa/(g/cm³), respectively, and a specific high strain rate compressive strength of 81.2 and 76.1 MPa/(g/cm³), respectively.
- The failure at high strain rate is initiated from the particle cracking and shear band formation in the matrix. A large compressive strain can be obtained in syntactic foams before densification because of a high volume fraction of porosity in the microstructure.
- The DMA testing showed that the storage modulus of syntactic foams is lower than that of the matrix alloy. It is also observed that the storage modulus of alloy decreases rapidly above a transition temperature, whereas the rate of decrease of storage modulus was nearly the same for syntactic foams in the test temperature range. Syntactic foams had a higher loss modulus than the matrix alloy at low temperatures. Due to the lack of viscoelasticity in metals, the storage modulus of the alloy was nearly the same as the elastic modulus and the loss modulus was comparatively negligible (two orders of magnitude lower).
- Syntactic foams had lower CTE compared to the matrix alloy. The syntactic foam demonstrated a higher CTE values at higher temperature.

Acknowledgments

This research is sponsored by the U.S. Army Research Laboratory contract W911NF-10-2-0084 of DST and the Cooperative Agreement W911NF-11-2-0096 with NYU. James was supported in part by the National Science Foundation under a GK-12 Fellows grant DGE-0741714: Applying Mechatronics to Promote Science. The program was also supported in part by the Central Brooklyn STEM Initiative (CBSI), which is funded by the Black Male Donor Collaborative, Brooklyn Community Foundation, J.P. Morgan Chase Foundation, Motorola Innovation Generation Grant, NY Space Grant Consortium, Xerox Foundation, and White Cedar Fund. Steven E. Zeltmann is thanked for help in manuscript preparation.

Author Contributions

James Cox, Dung D. Luong and Vasanth, Vasanth Chakravarthy Shunmugasamy contributed to the experimental research work and analysis. Oliver M. Strbik III manufactured the particles and syntactic foam specimens. Nikhil Gupta and Kyu Cho contributed to the analysis of results.

Conflicts of Interest

The authors declare no conflict of interest.

References

1. Ferguson, J.B.; Santa Maria, J.A.; Schultz, B.F.; Rohatgi, P.K. Al–Al₂O₃ syntactic foams—Part II: Predicting mechanical properties of metal matrix syntactic foams reinforced with ceramic spheres. *Mater. Sci. Eng. A* **2013**, *582*, 423–432.
2. Balch, D.K.; Dunand, D.C. Load partitioning in aluminum syntactic foams containing ceramic microspheres. *Acta Mater.* **2006**, *54*, 1501–1511.
3. *Metal Matrix Syntactic Foams: Processing, Microstructure, Properties and Applications*; Gupta, N., Rohatgi, P.K., Eds.; DEStech Publications: Lancaster, PA, USA, 2014.
4. Bardella, L.; Genna, F. On the elastic behavior of syntactic foams. *Int. J. Solids Struct.* **2001**, *38*, 7235–7260.
5. Bardella, L.; Sfreddo, A.; Ventura, C.; Porfiri, M.; Gupta, N. A critical evaluation of micromechanical models for syntactic foams. *Mech. Mater.* **2012**, *50*, 53–69.
6. Liu, J.A.; Yu, S.R.; Huang, Z.Q.; Ma, G.; Liu, Y. Microstructure and compressive property of in situ Mg₂Si reinforced Mg-microballoon composites. *J. Alloys Compd.* **2012**, *537*, 12–18.
7. Balch, D.K.; O'Dwyer, J.G.; Davis, G.R.; Cady, C.M.; Gray, G.T., III; Dunand, D.C. Plasticity and damage in aluminum syntactic foams deformed under dynamic and quasi-static conditions. *Mater. Sci. Eng. A* **2005**, *391*, 408–417.
8. Goel, M.D.; Peroni, M.; Solomos, G.; Mondal, D.P.; Matsagar, V.A.; Gupta, A.K.; Larcher, M.; Marburg, S. Dynamic compression behavior of cenosphere aluminum alloy syntactic foam. *Mater. Des.* **2012**, *42*, 418–423.

9. Luong, D.D.; Strbik, O.M., III; Hammond, V.H.; Gupta, N.; Cho, K. Development of high performance lightweight aluminum alloy/SiC hollow sphere syntactic foams and compressive characterization at quasi-static and high strain rates. *J. Alloys Compd.* **2013**, *550*, 412–422.
10. Gupta, N.; Luong, D.D.; Cho, K. Magnesium matrix composite foams—density, mechanical properties, and applications. *Metals* **2012**, *2*, 238–252.
11. Luong, D.D.; Shunmugasamy, V.C.; Gupta, N.; Lehmus, D.; Weise, J.; Baumeister, J. Quasi-static and high strain rates compressive response of iron and Invar matrix syntactic foams. *Mater. Des.* **2015**, *66 Part B*, 516–531.
12. Peroni, L.; Scapin, M.; Avalle, M.; Weise, J.; Lehmus, D. Dynamic mechanical behavior of syntactic iron foams with glass microspheres. *Mater. Sci. Eng. A* **2012**, *552*, 364–375.
13. Jha, N.; Mondal, D.P.; Goel, M.D.; Majumdar, J.D.; Das, S.; Modi, O.P. Titanium cenosphere syntactic foam with coarser cenosphere fabricated by powder metallurgy at lower compaction load. *Trans. Nonferrous Metals Soc. China* **2014**, *24*, 89–99.
14. Mondal, D.P.; Majumder, J.D.; Jha, N.; Badkul, A.; Das, S.; Patel, A.; Gupta, G. Titanium-cenosphere syntactic foam made through powder metallurgy route. *Mater. Des.* **2012**, *34*, 82–89.
15. Daoud, A. Effect of strain rate on compressive properties of novel Zn₁₂Al based composite foams containing hybrid pores. *Mater. Sci. Eng. A* **2009**, *525*, 7–17.
16. Taherishargh, M.; Belova, I.V.; Murch, G.E.; Fiedler, T. Low-density expanded perlite–aluminium syntactic foam. *Mater. Sci. Eng. A* **2014**, *604*, 127–134.
17. Licitra, L.; Luong, D.D.; Strbik, O.M., III; Gupta, N. Dynamic properties of alumina hollow particle filled aluminum alloy A356 matrix syntactic foams. *Mater. Des.* **2015**, *66*, 504–515.
18. Goel, M.D.; Mondal, D.P.; Yadav, M.S.; Gupta, S.K. Effect of strain rate and relative density on compressive deformation behavior of aluminum cenosphere syntactic foam. *Mater. Sci. Eng. A* **2014**, *590*, 406–415.
19. Mondal, D.P.; Das, S.; Ramakrishnan, N.; Bhasker, K.U. Cenosphere filled aluminum syntactic foam made through stir-casting technique. *Compos. Part A* **2009**, *40*, 279–288.
20. Orbulov, I.N. Compressive properties of aluminium matrix syntactic foams. *Mater. Sci. Eng. A* **2012**, *555*, 52–56.
21. Castro, G.; Nutt, S.R.; Wenchen, X. Compression and low-velocity impact behavior of aluminum syntactic foam. *Mater. Sci. Eng. A* **2013**, *578*, 222–229.
22. Maria, J.A.S.; Schultz, B.F.; Ferguson, J.B.; Rohatgi, P.K. Al–Al₂O₃ syntactic foams—Part I: Effect of matrix strength and hollow sphere size on the quasi-static properties of Al–A206/Al₂O₃ syntactic foams. *Mater. Sci. Eng. A* **2013**, *582*, 415–422.
23. Altenaiji, M.; Guan, Z.W.; Cantwell, W.J.; Zhao, Y.; Schleyer, G.K. Characterisation of aluminium matrix syntactic foams under drop weight impact. *Mater. Des.* **2014**, *59*, 296–302.
24. Zou, L.C.; Zhang, Q.; Pang, B.J.; Wu, G.H.; Jiang, L.T.; Su, H. Dynamic compressive behavior of aluminum matrix syntactic foam and its multilayer structure. *Mater. Des.* **2013**, *45*, 555–560.
25. Rohatgi, P.K.; Gupta, N.; Alaraj, S. Thermal expansion of aluminum–fly ash cenosphere composites synthesized by pressure infiltration technique. *J. Compos. Mater.* **2006**, *40*, 1163–1174.

26. Liang, X.; Li, H.J.; Yu, W.; Jing, X. A numerical simulation on the coefficient of thermal expansion of hollow particle filled resin syntactic foam. *Acta Metall Sinica* **2013**, *30*, 233–239.
27. Shunmugasamy, V.; Zeltmann, S.; Gupta, N.; Strbik, O., III. Compressive characterization of single porous SiC hollow particles. *J. Miner. Metals Mater. Soc.* **2014**, *66*, 892–897.
28. Gray, G.T., III. *Mechanical Testing and Evaluation*; ASM Handbook; ASM International: Materials Park, OH, USA, 2000; Volume 8.
29. Gupta, N.; Luong, D.D.; Rohatgi, P.K. A method for intermediate strain rate compression testing and study of compressive failure mechanism of Mg-Al-Zn alloy. *J. Appl. Phys.* **2011**, *109*, 103512.
30. Labella, M.; Shunmugasamy, V.C.; Strbik, O.M., III; Gupta, N. Compressive and thermal characterization of syntactic foams containing hollow silicon carbide particles with porous shell. *J. Appl. Polym. Sci.* **2014**, *131*, 1–5.
31. Wu, G.H.; Dou, Z.Y.; Sun, D.L.; Jiang, L.T.; Ding, B.S.; He, B.F. Compression behaviors of cenosphere–pure aluminum syntactic foams. *Scr. Mater.* **2007**, *56*, 221–224.
32. Rohatgi, P.K.; Kim, J.K.; Gupta, N.; Alaraj, S.; Daoud, A. Compressive characteristics of A356/fly ash cenosphere composites synthesized by pressure infiltration technique. *Compos. Part A* **2006**, *37*, 430–437.
33. Májlínger, K.; Orbulov, I.N. Characteristic compressive properties of hybrid metal matrix syntactic foams. *Mater. Sci. Eng. A* **2014**, *606*, 248–256.
34. Rivero, G.A.R.; Schultz, B.F.; Ferguson, J.B.; Gupta, N.; Rohatgi, P.K. Compressive properties of Al-A206/SiC and Mg-AZ91/SiC syntactic foams. *J. Mater. Res.* **2013**, *28*, 2426–2435.
35. Orbulov, I.N.; Májlínger, K. Description of the compressive response of metal matrix syntactic foams. *Mater. Des.* **2013**, *49*, 1–9.
36. Surappa, M.K. Synthesis of fly ash particle reinforced A356 Al composites and their characterization. *Mater. Sci. Eng. A* **2008**, *480*, 117–124.
37. Daoud, A.; Abou El-khair, M.T.; Abdel-Aziz, M.; Rohatgi, P. Fabrication, microstructure and compressive behavior of ZC63 Mg–microballoon foam composites. *Compos. Sci. Technol.* **2007**, *67*, 1842–1853.
38. Huang, Z.; Yu, S.; Li, M. Microstructures and compressive properties of AZ91D/fly-ash cenospheres composites. *Trans. Nonferrous Metals Soc. China* **2010**, *20* (Suppl. 2), s458–s462.
39. Guo, R.Q.; Rohatgi, P.K.; Nath, D. Preparation of aluminium-fly ash particulate composite by powder metallurgy technique. *J. Mater. Sci.* **1997**, *32*, 3971–3974.
40. Rohatgi, P.K.; Daoud, A.; Schultz, B.F.; Puri, T. Microstructure and mechanical behavior of die casting AZ91D-Fly ash cenosphere composites. *Compos. Part A* **2009**, *40*, 883–896.
41. Dou, Z.Y.; Jiang, L.T.; Wu, G.H.; Zhang, Q.; Xiu, Z.Y.; Chen, G.Q. High strain rate compression of cenosphere-pure aluminum syntactic foams. *Scr. Mater.* **2007**, *57*, 945–948.
42. Das, T.; Bandyopadhyay, S.; Blairs, S. DSC and DMA studies of particulate reinforced metal matrix composites. *J. Mater. Sci.* **1994**, *29*, 5680–5688.
43. Zhang, J.; Perez, R.J.; Lavernia, E.J. Effect of SiC and graphite particulates on the damping behavior of metal matrix composites. *Acta Metall. Mater.* **1994**, *42*, 395–409.
44. Zhang, J.; Perez, R.J.; Gupta, M.; Lavernia, E.J. Damping behavior of particulate reinforced 2519 Al metal matrix composites. *Scr. Metall. Mater.* **1993**, *28*, 91–96.

45. Davis, J.R. *Aluminum and Aluminum Alloys*; ASM Specialty Handbook; ASM International: Materials Park, OH, USA, 1993; pp. 1–784.
46. Labella, M.; Zeltmann, S.E.; Shunmugasamy, V.C.; Gupta, N.; Rohatgi, P.K. Mechanical and thermal properties of fly ash/vinyl ester syntactic foams. *Fuel* **2014**, *121*, 240–249.
47. Elomari, S.; Boukhili, R.; Lloyd, D.J. Thermal expansion studies of prestrained Al₂O₃/Al metal matrix composite. *Acta Mater.* **1996**, *44*, 1873–1882.

© 2014 by the authors; licensee MDPI, Basel, Switzerland. This article is an open access article distributed under the terms and conditions of the Creative Commons Attribution license (<http://creativecommons.org/licenses/by/4.0/>).